Operando Characterization of Catalysts through use of a Portable Microreactor

Shen Zhao,[a, b] Yuanyuan Li,[c] Eli Stavitski,[d] Ryan Tappero,[d] Stephen Crowley,[e] Marco J. Castaldi,[e] Dmitri N. Zakharov,[b] Ralph G. Nuzzo,[a] Anatoly I. Frenkel,*[c] and Eric A. Stach*[b]

In order to more deeply understand the mechanisms of catalytic reactions, improved methods are needed to monitor changes that occur in the electronic, structural, and chemical properties of catalytic systems under the conditions in which they work. We describe here a microreactor-based approach that integrates the capabilities of advanced X-ray, electron, optical, and gas-phase compositional analysis techniques under operando conditions. For several exemplary catalytic systems, we demonstrate how this approach enables the characterization of three of the major factors that contribute to structure–property correlations in heterogeneous catalysis. Specifically, we describe how this approach can be used to better understand the atomic structure and elemental composition of nanocatalysts, the physiochemical properties of the support and catalyst/support interfaces, and the gas- and surface-phase chemistry that occurs under operando conditions. We highlight the generality of the approach, as well as opportunities for future developments.

Introduction

In recent years, there has been an acceleration of experimental methods to probe the mechanisms of action that mediate heterogeneously catalyzed chemical reactions. These studies have yielded a more vibrant picture of the dynamic structural complexities that are found in such systems. It is now understood, for example, that structure is a feature of heterogeneous catalysts that is subject to change during the chemical transformations that occur under the high-temperature and pressure conditions at which most catalytic processes operate. The fundamental features of such forms of dynamic, operation-specific

[a] Dr. S. Zhao, Prof. R. G. Nuzzo
Department of Chemistry, University of Illinois
Urbana, IL 61801 (USA)

[b] Dr. S. Zhao, Dr. D. N. Zakharov, Dr. E. A. Stach
Center for Functional Nanomaterials
Brookhaven National Laboratory
Upton, NY 11793 (USA)
E-mail: estach@bnl.gov

[c] Dr. Y. Li, Prof. A. I. Frenkel
Department of Physics, Yeshiva University
New York, NY 10016 (USA)
E-mail: anatoly.frenkel@yu.edu

[d] Dr. E. Stavitski, Dr. R. Tappero
Photon Sciences Division
Brookhaven National Laboratory
Upton, NY 11973 (USA)

[e] S. Crowley, Prof. M. J. Castaldi
Department of Chemical Engineering
City College of New York
New York, NY 10031 (USA)

ORCID(s) from the author(s) for this article is/are available on the WWW under http://dx.doi.org/10.1002/cctc.201500688.

This publication is part of a Special Issue on "Advanced Microscopy and Spectroscopy for Catalysis". Once the full issue has been assembled, a link to its Table of Contents will appear here.

transformations are only now beginning to be understood. This highlights an important opportunity for the development of new methods of characterization applicable to the study of heterogeneous catalysts.[1] "Restructuring" commonly refers to the changes that occur in the bonding and composition of a nanocatalyst, and operando-mediated transformations of this type might result in changes in the bonding environments of either near-surface atoms (most common), the catalyst cluster shape, and perhaps most importantly the compositional motif (for example, random alloy to core–shell) of individual metal nanoparticles (NPs).[2] Notably, most heterogeneous catalysts— and even the well-defined model systems used to study them—are not single-phase/elementary composition solids, but rather they are present as a system that comprises distributions of size and composition. This structural heterogeneity can be quite important to the chemistry that the catalytic system supports. In this context, operando forms of restructuring can either lead to or be accompanied by changes in the overall properties of these ensembles, for example, size, shape, and degree of crystalline order.[3] These changes are caused either by: 1) interactions between the metal and the support and/or 2) interactions that result from the catalytic reaction itself, which include the formation, adsorption, desorption, and decomposition of reactants, intermediates, and products. Different experimental techniques have been developed to probe such aspects of heterogeneous catalytic processes, and significant emphasis has been placed on experimental and theoretical methods that address the atomistic underpinnings of the mechanisms of action. Even so, the ability to unify various forms of measurement within a common description of a mechanism remains limited. If we take as an example studies of supported transition-metal nanoscale catalysts, TEM is able

to elucidate features related to the morphology, crystal structure and composition, and (in select elements) the nature of the electronic structure of individual nanoparticles, as well as to provide a statistical overview of the relative distribution of NP size, composition and morphology.[4] X-ray absorption spectroscopy (XAS) describes both the electronic state of the nanoparticles (through the use of the X-ray absorption near-edge structure analysis; XANES) and the size, shape, and atomic arrangements of an "average particle" (through analysis of the extended X-ray absorption fine structure spectroscopy; EXAFS).[5] Electron energy loss spectroscopy (EELS)[6] probes the electronic structure and composition of both the metal NP and the support, and thus can be used to probe metal–support interactions in distinguishing and atomistically rationalized ways. Raman spectroscopy[7] can provide information about the chemical state and molecular vibrations that occur in oxide supports and thus can probe transformations in the structure of the support that can occur under reaction conditions. Finally, IR spectroscopy, gas chromatography–mass spectrometry (GC-MS), and residual gas analysis (RGA) can all be used to describe the gas-phase and surface species of reactants, intermediates, and products during catalytic reactions.[8]

However, further progress can only be addressed through the development of more accurate atomistic descriptions that overcome the limitations of "ensemble-averaging" structural methods and the requirements for measurement environments that weakly, if at all, replicate those found in a real process environment. If we take EXAFS as an example, the picture of an "average particle" that emerges from coordination-number modeling[5,9] may not represent an ensemble if the distribution of particle sizes and/or compositions is broad[9f,10] and/or if strongly asymmetric bonds (which are typical for strained nanoparticle surfaces because of intrinsic relaxation or bonding interactions with adsorbates) are present.[11] Recent EXAFS experiments with nanoscale metal catalysts (both mono- and bimetallic) have demonstrated the limitations of this approach in documenting the nature of the structural and compositional habits embedded in even the relatively simple ensembles found within model systems.[10c,11a] If the distribution of composition or size/shapes is broad, experimental artifacts can cause an underestimation of the average particle size[11c] or compositional motifs (for example, random alloy NPs can be mistaken for core–shell NPs).[10b] In addition—and most importantly—catalytic materials are subject to reaction-driven forms of transformation, in which the sizes and compositions of catalytic NPs can change dynamically under reaction conditions.[12] These properties of catalysts highlight the need to include a method such as scanning transmission electron microscopy (STEM)/TEM, which can provide useful statistical analysis of particle size, shape, and composition as a means to describe the ensemble attributes of the structure present in a catalytic material, as well as the structural and compositional transformation that might occur during chemical reactions.[13]

The capabilities that such methods engender notwithstanding, there remains a more fundamental impediment to the advancement of methods of characterization, namely, the static nature of many experimental methods that offer capabilities to probe the structure at atomic resolution. The techniques described above are often performed ex situ and/or ex post-facto, and thus provide information about the initial and/or final stages of the reaction, and thus likely miss features crucial to understand changes that may occur dynamically during the catalytic cycle. The characteristics of operation at elevated temperatures and pressures (conditions that are typical for many reactions catalyzed heterogeneously used in the synthesis of fuels and chemicals) as well as specific changes to the process stream feeds can provide strong thermodynamic driving forces that change the structure and composition of both the metal NP catalysts and their supports and drive reactions along distinct chemical pathways.[3b,14] Importantly, the intermediate states of the catalysts, overlooked by static measurements, may be the catalytically active ones or at least add to the understanding of the reaction sequence. For these reasons and to understand reaction mechanisms in contexts that are explicitly relevant to operational conditions, it is imperative to follow transformation kinetics both in real time and under operando conditions. These points frame goals that stand as grand challenges that we need to address to foster progress in this important field of research: these factors drive the increasing emphasis given to so-called in situ and operando techniques in studies of supported catalysts.[15] In the case of in situ characterization, the exposure of the sample to more relevant physical conditions (such as at elevated temperatures or pressures) are made in an effort to better mimic real process states. These in situ techniques—although they help to elucidate some features of important structure–property correlations—miss an important element, namely, that of function. An understanding of structure is of course important, but it remains less useful if not coupled in a clear way to how molecular constituents are transformed by the reactions that occur within the system. Without the detection of the products of a catalytic reaction, the relevance of the structural characterization, even if performed in situ, to a mechanistic understanding of reaction kinetics is unquestionably lost. During an operando characterization, the relevant characterization approach is applied while the catalysts are held "under working conditions", as validated by measurements of the activity, selectivity, and/or stability of the catalyst. Operando characterization is perhaps the most ideal form of characterization of functional materials, not only because it ensures that the measured parameters properly describe the system as it functions but also because it allows direct links to be made between different experiments performed under equivalent conditions.[16]

The importance of operando characterization is now broadly accepted, and there have been significant developments in the modes of experiments made in this regard. As examples, techniques such as XAS,[17] XRD,[18] Raman spectroscopy,[19] UV/Vis spectroscopy,[20] and IR spectroscopy[21] have all been utilized within operando modes of characterization to study working catalytic systems. These techniques benefit from the low-scattering cross-sections of photons with matter, which allow deep penetration into materials and simplify the types of reactor designs that can be utilized for operando characterization. Techniques such as TEM, X-ray photoelectron spectrosco-

py (XPS), and scanning tunneling microscopy (STM) are more challenging to perform under ambient or even harsh reaction conditions because of the extremely limited travelling distance of electrons through moderate-pressure or even low-vacuum atmospheres. These techniques normally require high vacuum or ultra-high vacuum (UHV) to function effectively. Although differential pumping can provide locally increased pressure environments to the sample, this approach cannot close the so-called the "pressure gap" entirely. It has not been possible, even until very recently, to bridge this gap and fully reproduce reactions within an integrated protocol that exploits all of these important modes of experimental characterization.

As the natures of reactions catalyzed heterogeneously can differ dramatically, there are different types of operando studies that have been developed for use within specific fields of research such as electrochemistry,[22] catalysis,[23] and surface science.[24] It has been generally accepted that multiple probes are required to characterize complementary attributes of catalytic systems, but implementations of this understanding within experiments have varied from group to group.[23, 25] Recently, Levin and Billinge proposed an approach in which available data and theoretical modeling results are optimized to solve a general nanostructure problem.[26] For use within structural and mechanistic studies in catalysis, a limitation exists in the data taken from different instruments often must be measured under a variety of physicochemical states (for example, some ex situ, some in situ, and some operando conditions). The correlation of such measurements is challenging because they may probe completely different states of, and possibly completely different forms of, materials systems. An alternative approach of interest in our work is one that makes it possible to perform all operando characterization methods across multiple instrumental platforms while maintaining and/or manipulating the sample under identical physicochemical states. Although this approach addresses the limitation of that proposed by Levin and Billinge, it suffers from a different problem: techniques such as TEM, XPS, and STEM cannot be combined with X-ray and other probes, which thereby limits the scope of the problems that might be solved in this way.[23]

Recent development of micromachined, enclosed cell reactors (microcells) has enabled operando TEM studies of catalytic reactions in the ambient atmosphere. With reaction volumes reduced to approximately 10^{-5} mm^3, which lead to much lower transport resistance and rates of conversion and much faster heat and mass transfer rates as a result, microcells offer distinct advantages in catalytic reaction studies compared to bulk reactors.[27] TEM investigations, now possible under atmospheric pressure because of the closed-cell approach and thin window materials, can provide missing information about the size, shape, and composition of the nanomaterials under operando conditions[28] and hence, can be used as a unique platform to combine operando characterization of the same catalytic process analyzed by using different instruments under identical reaction conditions. To illustrate this approach in our previous work, we described the use of a microreactor for correlated studies of Pt catalysts during ethylene hydrogenation by combined XAFS and TEM.[12]
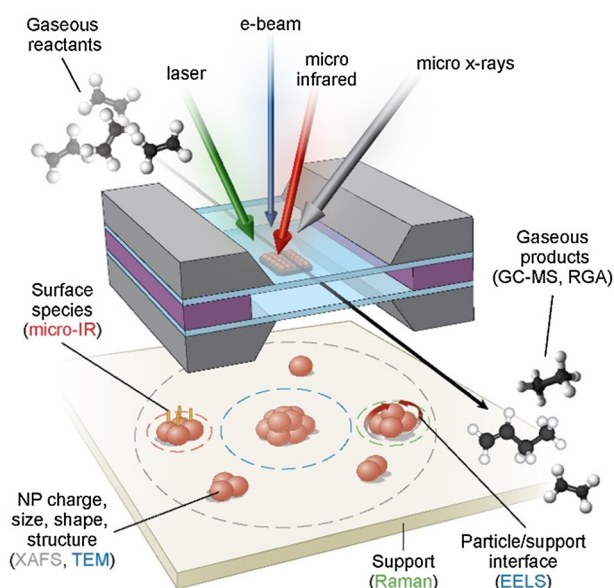

Figure 1. Schematic of the microcell. The catalyst is confined between two silicon nitride windows, and the reaction gases flow through the system to interact with the confined catalyst at atmospheric pressure. We show how the four different beams (electron, X-ray, IR, and laser) probe different parts of the catalytic system.

Here we show, through representative examples, how we used this microcell-enabled method of characterization to illuminate the two basic structure–property correlations that involve heterogeneous catalysts. The essence of our method is illustrated in Figure 1: the same reaction was studied at each facility (synchrotron, electron microscope, etc.) in the same microreactor, while we probed the reactivity simultaneously by using an online residual gas analyzer. To this end, X-ray and IR microspectroscopy experiments were conducted at the National Synchrotron Light Source (NSLS) and STEM/EELS measurements were performed at the Center for Functional Nanomaterials (CFN) both at Brookhaven National Laboratory. GC–MS measurements were conducted at the City College of New York (CCNY). The formation of reaction products was detected at each facility and was used to correlate the data from each instrument, as measured at the same stages of the reaction. Ethylene hydrogenation (and as we show, the concomitant formation of oligomers that are retained by and over time modify the properties of the support) and CO oxidation were chosen as exemplary catalytic reactions and processes for proof-of-principle demonstrations of the integrated microreactor capabilities of interest in this work. STEM, EELS, and XAS characterizations were used to obtain structural and electronic information pertaining to the catalyst and support. IR microspectroscopy and Raman spectroscopy were used to identify the surface products of the catalysis and support properties, respectively. GC–MS and RGA (MS) were used for detailed gas-phase analysis. How the different experimental approaches described above probe different portions of the catalytic system are shown schematically in Figure 1, which highlights the versatility of this new approach.

We present an overview of the design of the microreactor used to integrate this specific multiplatform method of measurement and the data it affords using these individual tests. We discuss extensions that can be envisioned that would serve to further its use within measurements that exploit both the advanced and developing capabilities of synchrotron sources.

Results and Discussion

In this section we present results of exemplary experiments performed in the microreactor, grouped according to a particular aspect of a catalytic system they illuminate, namely, 1) the structure and electronic properties of metal catalysts, 2) the nature of the support, and 3) the catalytic chemistry. Notably, as a result of the extremely small window area of the microcell (50×50 µm), we need to take advantage of microfocused X-ray and IR beams for all XANES, EXAFS, and IR experiments.

Figure 2. STEM images that show Pt-SiO$_2$ NPs during different reaction regimes, a) pure H$_2$; b) H$_2$/C$_2$H$_4$ = 3:1; c) pure H$_2$; d) H$_2$/C$_2$H$_4$ = 1:3; e) pure H$_2$ under 1 atm pressure; f) mean particle size under all five reaction regime (only particles that do not touch each other were counted). All images were taken at room temperature after the gas flow through the reactor stabilized (≈2 h).[12] The electron dose rate was 600 e⁻/Å^2 s.

Metal catalysts

In this section we present results concerning the chemical state, structure, and statistical distribution of particle sizes of supported Pt and Au catalysts by STEM, XANES, and EXAFS.

STEM

STEM analysis can provide accurate size information to study the morphology and size distribution of metal NPs. Direct visualization of the size, shape, and dispersion of the metal NPs before a reaction is used commonly to describe the initial morphology of the system following catalyst preparation, whereas ex post-facto measurements are used commonly to observe the cumulative changes that occur as a result of the reaction. Additionally, by obtaining the data under operando conditions, these electron microscopy (EM) images are able to give statistical information of how these NPs transform (sintering, ripening, and fragmentation) during the actual catalytic cycle. Compared with techniques such as XAS, which often provide average particle information, STEM images provide local particle information, which can be critical because of the heterogeneity frequently observed in NP systems.

STEM analysis of the particle size distribution and changes in the mean particle sizes of Pt-SiO$_2$ during the flow of H$_2$ and C$_2$H$_4$ at different volumetric ratios are shown in Figure 2.[12] These STEM images were recorded at 1 atm pressure. Different stages of the reaction identified in this experiment yield de-
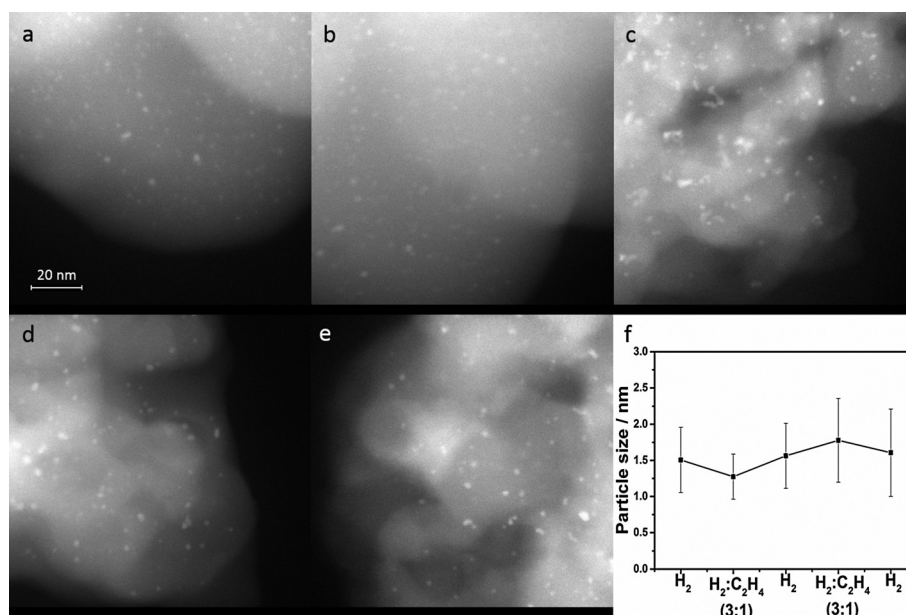
tailed information on the size and shape of the Pt NPs that change under the reaction conditions.[12] For example, after the second H$_2$ flow step is reached, following the first C$_2$H$_4$ hydrogenation step, a significant number of dumbbell-shaped particles were observed, which strongly suggests that motion of the particles on the substrate occurred and indicates the initial stages of sintering (Figure 2c). Interestingly, if the sample was returned to C$_2$H$_4$-rich conditions (Figure 2d), these larger agglomerate particles were seen to fracture and form smaller clusters again. A detailed discussion of the origins of these and related phenomena can be found in our previous work.[12] For the purpose of this report, we would like to emphasize the following points: it is possible to obtain a high-quality, statistically significant sample of particle size and shape throughout the reaction sequence under all atmospheric pressures of reactive streams. The fact that these observations can be made in significantly rich hydrocarbon streams is both surprising and important. Hydrocarbons often lead to significant contamination during EM imaging, yet we found that with appropriate considerations of the dose and dose rate, it was possible to obtain images with <1 nm resolution, even under atmospheric pressures. Observations such as these demonstrate clearly the utility of the microcell approach for operando STEM imaging.

XANES

XANES can provide information regarding the electronic structure of metal catalysts. As we can analyze the features caused by electronic transitions to empty bound states, XANES is often used to determine both the chemical state and the bonding characteristics of the metal. A comparison of Au L$_3$-edge XANES data measured from titania-supported Au NPs
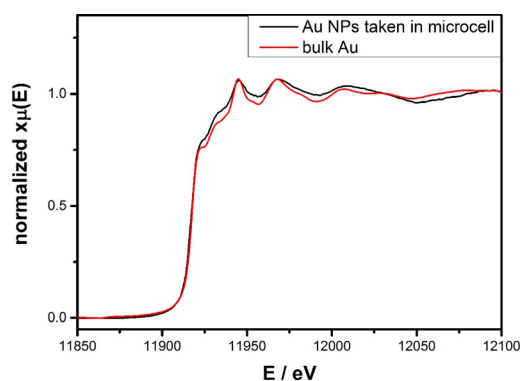
Figure 3. XANES spectra at Au L$_3$-edge between microcell data for TiO$_2$ supported Au NPs and bulk Au foil.

and bulk Au foil is shown in Figure 3. The NP data were collected in the microreactor under ambient conditions. The Au NPs have an average size of 4 nm and show metallic XANES features, very similar to bulk Au.

EXAFS

EXAFS is a local structure probe based on the analysis of the oscillations of the X-ray absorption coefficient that extend to approximately 1000–1500 eV above the absorption edge of an X-ray-absorbing atom. This technique can provide structural information such as the distance between the neighboring atoms, their coordination numbers, and bond length disorder, as well as the changes in these quantities under different reaction regimes. Fourier-transformed magnitudes of EXAFS data collected from Au NPs supported on Al$_2$O$_3$ are shown in Figure 4. The spectra were collected during the flow of a mixture of CO and O$_2$ (1:10 ratio) and in He before and after the gas mixture flow. One can see irreversible changes in the intensity of the peaks in the range of 2–3.4 Å that occurred during the gas mixture flow, possibly because of changes in the metal–metal coordination numbers and, hence, the irreversible growth of Au NPs.
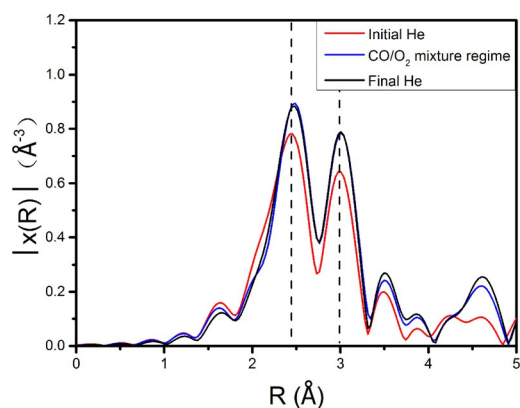

Figure 4. Fourier transform magnitudes of Au L$_3$-edge k^2-weighted EXAFS spectra measured in situ for Au-Al$_2$O$_3$ catalysts under flow of He and CO/O$_2$ (1:10).

Table 1. Best fit results for Au–Au coordination numbers (N), bond lengths (R), and their disorder (σ^2) in Au-Al$_2$O$_3$ under different atmospheric regimes obtained by EXAFS analysis of the data shown in Figure 4. The last column shows the correction to the photoelectron energy origin (ΔE_0).

Conditions	N_{Au-Au}	R_{Au-Au} [Å]	σ^2 [Å^2]	ΔE_0 [eV]
He initial	7.3 ± 0.9	2.846 ± 0.008	0.0062 ± 0.007	6.8 ± 0.6
CO and O$_2$	8.9 ± 1.1	2.867 ± 0.006	0.0062 ± 0.007	6.8 ± 0.6
He final	8.9 ± 1.0	2.867 ± 0.006	0.0062 ± 0.007	6.8 ± 0.6

Quantitative data analysis (Table 1) confirmed this hypothesis. Data were analyzed by conventional procedures by using the IFEFFIT data analysis package and FEFF6 code.[29] Coordination numbers, correction to Au–Au distances, and their disorders were varied in the fits, together with the correction to the photoelectron energy origin. The latter parameters were constrained to be the same for all three data sets to minimize the correlation of the fitting parameters.

In summary, we have shown how both STEM and XAS can be used to quantify the electronic and structural information of metal catalysts during realistic in situ and operando conditions. The representative data quality is good, which thus enables quantitative analysis of catalysts during reaction conditions by these techniques.

Properties of catalytic supports

In this section we present results obtained by probing silica and titania supports using EELS and Raman spectroscopy.

EELS

EELS is an electron analogue to XAS, whereby a magnetic spectrometer is used to separate the electrons that have left the sample according to the energy that they have lost during inelastic interactions with atoms in the sample. Thus, it offers insights into the electronic structure of the target supporting materials in a manner that is analogous to XANES. In addition, it is possible to perform nanometer-scale chemical mapping using EELS (in either the STEM-EELS spectrum imaging mode or through so-called energy-filtered imaging; EFTEM). Thus, EELS can probe the composition and electronic structure of individual NPs, information that can be critical to understand the fundamental chemistry of catalytic reactions. Additionally, the catalytic properties of a system can depend greatly on the interface between the metal and the support: EELS has the potential to be able to observe electronic structure changes that occur in the supporting materials during a reaction directly and thus can describe such important effects as the interaction between the metal and support. Here we show just one example taken from the Si L-edge obtained under atmospheric pressure in the microcell for the Pt-SiO$_2$ sample. Importantly, the microcell consists of two SiN windows, and thus any contribution to the Si L-edges necessarily consists of a signal from the two membrane windows.
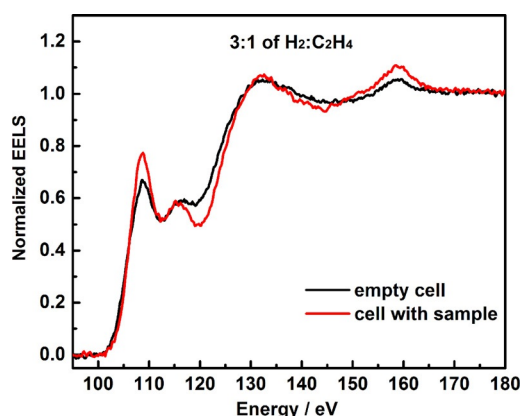
Figure 5. Operando EELS spectra of the Si L-edge under different reaction regimes. The individual spectra show differences in the near-edge structure that depend on the nature of the reactive environment.

Figure 6. Raman spectra of pure TiO_2 (anatase) taken in microcell and conventional tube reactor.

Changes in the Si EELS spectra collected during the flow of a 3:1 H_2/C_2H_4 mixture over Pt/SiO_2 catalysts in the ethylene hydrogenation experiment described in the previous section are shown in Figure 5. In addition to the spectrum obtained with the sample loaded in the cell, a spectrum obtained in a control experiment without the sample is shown to subtract the effect caused by the SiN windows. The two strong peaks at 108 and 115 eV are associated with Si—O bonds[30] that exhibit a transformation in response to the reaction conditions.

Raman spectroscopy

Raman spectroscopy provides fingerprints of molecules and/or crystal structures by probing their vibrational properties. Operando Raman spectroscopy was combined with XAS in the same experiments to correlate changes in catalysts with changes in support materials under the reaction conditions.[25a, 31] Raman spectroscopy can be used to determine the crystalline phase of different catalytic supports.[32] A comparison of representative Raman spectra for pure TiO_2 probed in the microreactor and in a larger (quartz capillary) tube reactor is shown in Figure 6. The positions of the Raman bands observed in the spectra from both cells are in good agreement with those expected for an anatase structure. The well-resolved peak at $\tilde{\nu} = 145$ cm^{-1} is assignable to the main anatase vibrational mode. In addition, modes at $\tilde{\nu} = 397$ (B_{1g}), 517 (A_{1g}), and 638 cm^{-1} (E_g) are seen in both spectra, which indicates that the majority of the sample was present in the crystalline form.[33]

The fact that both spectra show very similar features demonstrates the feasibility to employ the microcell for Raman measurements made both in situ and under operando conditions.

Catalytic chemistry

In this section we present exemplary data on detection of gas-phase and surface species formed during catalytic reactions.
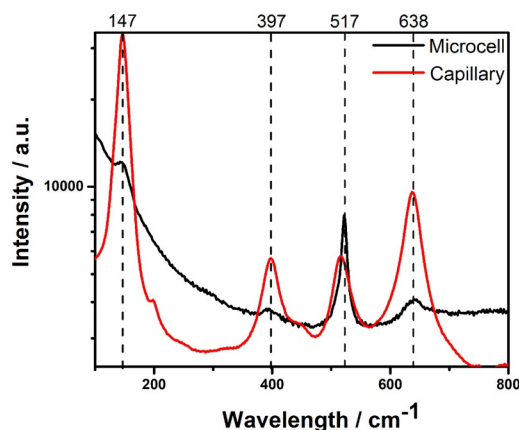
Surface catalytic intermediate and product analysis

IR spectroscopy is a powerful technique to perform surface analysis of adsorbates that can bind to both metals and supports. Operando IR spectroscopy can thus contribute vitally important data to understand the surface chemistry of a catalyst in real time. Time-resolved synchrotron IR microspectroscopy data obtained under the same conditions of the ethylene hydrogenation reaction experiment described above are presented in Figure 7. These data were measured for the stoichiomet-
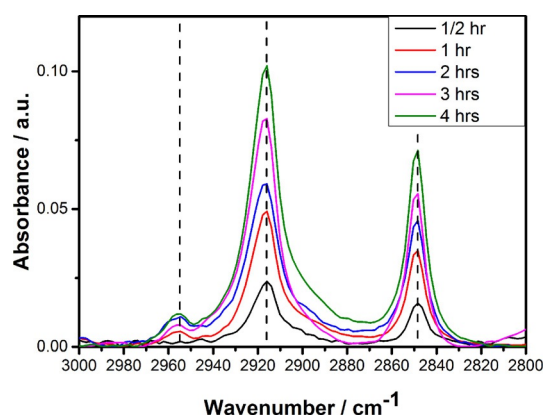

Figure 7. Time-resolved IR spectra collected during room-temperature ethylene hydrogenation over the Pt-SiO$_2$ catalyst.

ric reaction conditions ($H_2/C_2H_4 = 1:1$) as a function of time. These results show the direct formation and retention on the support of aliphatic hydrocarbon products formed during the ethylene hydrogenation process through a competing, and generally low yield, oligomerization pathway. The aliphatic speciation implied here is supported by the fact that the modes that appear in the C—H stretching region (the three peaks centered at $\tilde{\nu} = 2958$, 2918, and 2850 cm^{-1}) under operando reaction conditions can be assigned directly to the C—H stretching frequencies of (linear) hydrocarbons. The significant growth of the peaks at $\tilde{\nu} = 2918$ cm^{-1} (asymmetric CH_2 stretch) and $\tilde{\nu} =$

2850 cm^{-1} (symmetric CH$_2$ stretch) indicates that heavier oligomers are formed and accumulate on/within the support over time.

By examining the IR spectra taken in the microcell, we were able to detect subtle changes of the surface species that were formed on the Pt catalyst and/or support. The experiment illustrates the potential of this method to measure surface species (reactants, intermediates, and products) using the microcell.

Gas-phase catalytic product analysis

RGA and GC–MS can be used to identify and quantify gas-phase products and thus help in studies of catalytic reaction kinetics. Examples of their use are shown in Figures 8 and 9.
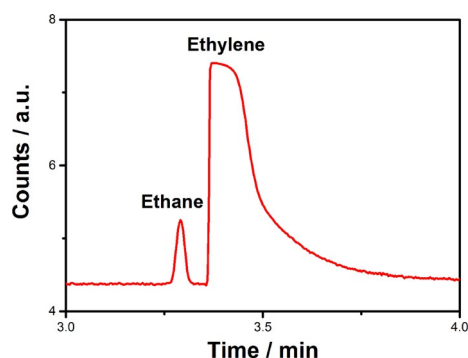

Figure 8. Gas chromatogram that shows the reactant (ethylene) and product (ethane) for ethylene hydrogenation over Pt-SiO$_2$.
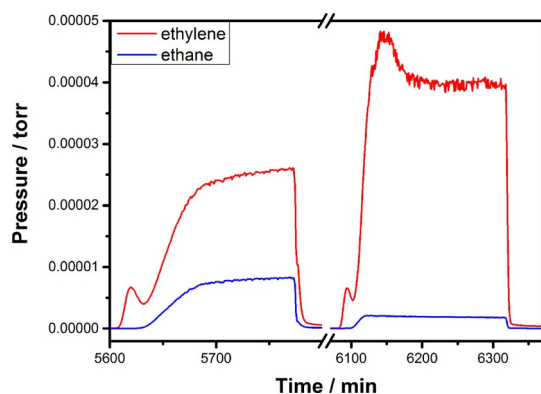

Figure 9. RGA data comparison that shows the pressure of the reactant (ethylene) and product (ethane) between H$_2$/C$_2$H$_4$ = 1:1 and pure ethylene.

The gas chromatogram of ethane and ethylene elution during ethylene hydrogenation over Pt-SiO$_2$ under stoichiometric reaction conditions (H$_2$/C$_2$H$_4$ = 1:1) is shown in Figure 8. The ethane and ethylene peaks were well separated. The irregular shape of the ethylene peak was a result of the large amount of ethylene in the GC sample loop, yet it was still quantifiable. As a result of the extremely small loading of the catalyst in the microcell, ethane production was low, but still yielded a significant signal-to-noise ratio. This demonstrates that GC–MS can

be utilized to measure gas-phase product formation directly from the microcell output.

RGA data were taken from the output of the microcell under the same conditions as used for the GC–MS experiment described above. Ethane production increases under ideal, stoichiometric reaction conditions (1:1 ratio of hydrogen to ethylene) compared to the baseline experiment in which pure ethylene was fed into the cell (Figure 9).

Both the GC–MS and RGA results show unambiguous evidence that catalytic ethylene conversion in the microcell can be detected by analyzing the gas-phase composition downstream of the cell. Both techniques provide valuable insights into the catalytic mechanism and kinetics of ethylene hydrogenation over the Pt-SiO$_2$ catalyst.

The above data collected in several proof-of-principle experiments demonstrate the ability of different techniques to probe a catalytic system in the microreactor. In most cases, these data were complemented by corresponding reaction data collected online in parallel with catalyst characterization. Our method, therefore, shows strong promise for combined, operando studies of catalytic reactions that circumvent the main limitations of existing approaches (ex situ combinations of all relevant methods[26] and in situ/operando combinations of multiple techniques in the same experiment[23a]). As a result of the improved heat and mass transfer and low conversion rates, microreactor studies of reaction kinetics have unique advantages over bulk reactors used in operando characterization.

With the further development and application of the microreactor and new methods of its integration with multiple experimental facilities, it is envisioned that this approach will see even broader utilization. Although all the results shown above have been obtained from catalyzed chemical reactions that occur at room temperature, recent developments in microcell fabrication have led to the creation of systems that can achieve quite high temperatures.[34] Nanoscale TEM and STEM imaging at temperatures as high as 800 °C have been achieved, and temperatures of 500 °C can be maintained in highly aggressive environments for many hours before heating element failure.

Additionally, there do not appear to be strong restrictions to the use of microfabricated reactors in a variety of additional experimental approaches relevant to the characterization of NP catalysts. These include bulk probes such as XRD and X-ray and electron-pair distribution function analysis, as well as focused, nanoprobe X-ray probes such as nanodiffraction and transmission X-ray and scanning transmission X-ray imaging. Importantly, quantitative stable gas-phase measurements can be obtained by RGA and GC–MS to understand the catalytic cycle fully. Furthermore, with the increasing development of the approach, it is possible that X-ray photoelectron spectroscopy may also be included in the characterization suite.[35]

Conclusion

The discussions above illustrate the scope and diversity of the forms of data that can be measured in integrated form using a common reactor microcell. Different types of microscopy

(scanning transmission electron microscopy) and spectroscopy (electron energy loss, X-ray absorption, IR, and Raman spectroscopy) were utilized to provide new insights into the nature of the structure–property relationships that exist in prototypical catalytic reactions under operando conditions. In this work, we selected ethylene hydrogenation and CO oxidation as exemplary reactions and we used them to demonstrate the unique qualities and inherent practicality of the integrated microcell methodology. This approach features a cell design that specifically enables the features needed for combined studies of this type and in ways that can be exploited for investigations of essentially any catalytic reaction under operando conditions. The highlights presented above, if taken together with our study reported recently on the mechanisms that operate in the dynamic transformation of supported Pt nanocluster catalysts during the ethylene hydrogenation reaction,[12] illustrate an approach that could in principle be applied as a general methodology within the broader field of operando research in heterogeneous catalysis.

Experimental Section

Cell design

The microcell consists of two 50×50 μm SiN windows with a 500 nm spacing in between connected to three capillary channels (inlet, outlet, and bypass). The catalyst was loaded between the two windows and reactants were introduced into the cell by using mass flow controllers (MFCs), and pressure controllers provided the desired pressure and steady flow rate. More details can be found at http://hummingbirdscientific.com/products/gas-flow/.

Experiments with the microreactor

Experiments with the microreactor are summarized below. These are grouped according to the experimental facility used. If appropriate, they are characterized as ex situ, in situ, or operando experiments.

To study real-time reactivity, mixtures of various feed gases (H_2 and C_2H_4 or CO and O_2) of variable compositions were flowed through the reactor cell. The pressure in the flow microcell was slightly above atmospheric pressure (1000 Torr).

Electron microscopy experiments were performed by using a Titan 80–300 environmental transmission electron microscope at the Center for Functional Nanomaterials, Brookhaven National Laboratory. Annular dark-field scanning transmission electron microscopy images were acquired at a constant image magnification of 640 000 times magnification operating at 300 keV.

The XANES and EXAFS measurements were performed at beamline X27A, National Synchrotron Light Source (NSLS). The microcell was mounted on the stage approximately 45° to the incident X-ray beam, and the emitted fluorescence was detected from the downstream side of the cell by using a four-channel Vortex detector. All XAFS spectra were recorded after the gases reached stable state.

The IR microspectroscopy experiments were performed by using the N_2-purged Thermo Nicolet Magna 860 Step-Scan FTIR and Spectra Tech Continuum IR Microscope at the U2B beamline (NSLS). The IR measurements were performed under a continuous gas flow with 4 cm^{-1} spatial resolution and 256 scans.

Raman spectra for all TiO_2 films were collected by using a Bay Spec spectrometer equipped with a 532 nm laser excitation. The spectrometer was calibrated using a silicon wafer to a wavenumber accuracy of ± 1 cm^{-1}. A noncontact fiber-optic HT probe objective was used for beam focusing and collection of scattered radiation. Five spectra were accumulated with a 30 s exposure time. The resulting total spectral recording time was 150 s. The laser output power was 23 mW.

An on-line GC–MS system (Agilent 7890A GC equipped with 5975c MS detector) equipped with a GS-GasPro column (Agilent 60 m × 0.32 mm) was used to analyze gas-phase compounds. He (UHP grade) was used as carrier gas in constant flow mode. The oven temperature was programmed from 40 to 150 °C at ramping rate of 20 °C min^{-1}, held at 150 °C for 1 min, then ramped to 200 °C at rate of 20 °C min^{-1} and held for 3 min. The temperature of the quad and source of MSD were 180 and 230 °C, respectively.

An RGA (SRS) was used to monitor the real-time mass production for CO oxidation reactions. It was connected to the outlet of the microcell for the experiments described above.

Keywords: heterogeneous catalysis · microreactors · operando spectroscopy and microscopy · structure–activity relationships · supported catalysts

[1] a) Y. G. Sun, Y. N. Xia, Science 2002, 298, 2176–2179; b) S. Polarz, A. Roy, M. Lehmann, M. Driess, F. E. Kruis, A. Hoffmann, P. Zimmer, Adv. Funct. Mater. 2007, 17, 1385–1391; c) K. Köhler, R. G. Heidenreich, S. S. Soomro, S. S. Prockl, Adv. Synth. Catal. 2008, 350, 2930–2936; d) J. Kugai, T. Moriya, S. Seino, T. Nakagawa, Y. Ohkubo, H. Nitani, T. A. Yamamoto, Int. J. Hydrogen Energy 2013, 38, 4456–4465.

[2] a) G. A. Somorjai, Y. Borodko, Catal. Lett. 1999, 59, 89–91; b) F. Tao, S. R. Zhang, L. Nguyen, X. Q. Zhang, Chem. Soc. Rev. 2012, 41, 7980–7993; c) F. Tao, M. E. Grass, Y. W. Zhang, D. R. Butcher, J. R. Renzas, Z. Liu, J. Y. Chung, B. S. Mun, M. Salmeron, G. A. Somorjai, Science 2008, 322, 932–934; d) S. Wunder, Y. Lu, M. Albrecht, M. Ballauff, ACS Catal. 2011, 1, 908–916.

[3] a) L. Li, L. L. Wang, D. D. Johnson, Z. F. Zhang, S. I. Sanchez, J. H. Kang, R. G. Nuzzo, Q. Wang, A. I. Frenkel, J. Li, J. Ciston, E. A. Stach, J. C. Yang, J. Am. Chem. Soc. 2013, 135, 13062–13072; b) T. W. Hansen, J. B. Wagner, ACS Catal. 2014, 4, 1673–1685; c) D. S. Su, B. S. Zhang, R. Schlogl, Chem. Rev. 2015, 115, 2818–2882; d) S. B. Vendelbo, C. F. Elkja-

er, H. Falsig, I. Puspitasari, P. Dona, L. Mele, B. Morana, B. J. Nelissen, R. van Rijn, J. F. Creemer, P. J. Kooyman, S. Helveg, *Nat. Mater.* **2014**, *13*, 884 – 890.

[4] a) Z. L. Wang, *Adv. Mater.* **2003**, *15*, 1497 – 1514; b) J. C. Yang, M. W. Small, R. V. Grieshaber, R. G. Nuzzo, *Chem. Soc. Rev.* **2012**, *41*, 8179 – 8194.

[5] a) A. I. Frenkel, *J. Synchrotron Radiat.* **1999**, *6*, 293 – 295; b) A. I. Frenkel, C. W. Hills, R. G. Nuzzo, *J. Phys. Chem. B* **2001**, *105*, 12689 – 12703.

[6] B. K. Miller, P. A. Crozier, *Microsc. Microanal.* **2014**, *20*, 815 – 824.

[7] I. E. Wachs, C. A. Roberts, *Chem. Soc. Rev.* **2010**, *39*, 5002 – 5017.

[8] a) A. Corma, L. T. Nemeth, M. Renz, S. Valencia, *Nature* **2001**, *412*, 423 – 425; b) P. Shen, S. Zhao, D. Su, Y. Li, A. Orlov, *Appl. Catal. B* **2012**, *126*, 153 – 160; c) I. E. Wachs, *Catal. Today* **1996**, *27*, 437 – 455.

[9] a) M. S. Nashner, A. I. Frenkel, D. L. Adler, J. R. Shapley, R. G. Nuzzo, *J. Am. Chem. Soc.* **1997**, *119*, 7760 – 7771; b) A. Jentys, *Phys. Chem. Chem. Phys.* **1999**, *1*, 4059 – 4063; c) S. Calvin, M. M. Miller, R. Goswami, S. F. Cheng, S. P. Mulvaney, L. J. Whitman, V. G. Harris, *J. Appl. Phys.* **2003**, *94*, 778 – 783; d) B. Roldan Cuenya, J. R. Croy, S. Mostafa, F. Behafarid, L. Li, Z. F. Zhang, J. C. Yang, Q. Wang, A. I. Frenkel, *J. Am. Chem. Soc.* **2010**, *132*, 8747 – 8756; e) A. Frenkel, *Z. Kristallogr.* **2007**, *222*, 605 – 611; f) A. I. Frenkel, *Chem. Soc. Rev.* **2012**, *41*, 8163 – 8178; g) A. M. Beale, B. M. Weckhuysen, *Phys. Chem. Chem. Phys.* **2010**, *12*, 5562 – 5574.

[10] a) G. Agostini, R. Pellegrini, G. Leofanti, L. Bertinetti, S. Bertarione, E. Groppo, A. Zecchina, C. Lamberti, *J. Phys. Chem. C* **2009**, *113*, 10485 – 10492; b) A. I. Frenkel, Q. Wang, S. I. Sanchez, M. W. Small, R. G. Nuzzo, *J. Chem. Phys.* **2013**, *138*; c) A. I. Frenkel, A. Yevick, C. Cooper, R. Vasic, *Annu. Rev. Anal. Chem.* **2011**, *4*, 23 – 39.

[11] a) S. T. Chill, R. M. Anderson, D. F. Yancey, A. I. Frenkel, R. M. Crooks, G. Henkelman, *ACS Nano* **2015**, *9*, 4036 – 4042; b) O. M. Roscioni, N. Zonias, S. W. T. Price, A. E. Russell, T. Comaschi, C. K. Skylaris, *Phys. Rev. B* **2011**, *83*; c) A. Yevick, A. I. Frenkel, *Phys. Rev. B* **2010**, *81*.

[12] Y. Li, D. Zakharov, S. Zhao, R. Teppero, U. Jung, A. Elsen, Ph. Baumann, R. G. Nuzzo, E. A. Stach, A. I. Frenkel, *Nat. Commun.* **2015**, *6*, 7583 – 7588.

[13] a) H. L. L. Xin, H. Alayoglu, R. Z. Tao, A. Genc, C. M. Wang, L. Kovarik, E. A. Stach, L. W. Wang, M. Salmeron, G. A. Somorjai, H. M. Zheng, *Nano Lett.* **2014**, *14*, 3203 – 3207; b) H. L. Xin, E. A. Pach, R. E. Diaz, E. A. Stach, M. Salmeron, H. M. Zheng, *ACS Nano* **2012**, *6*, 4241 – 4247.

[14] a) D. Gamarra, G. Munuera, A. B. Hungria, M. Fernandez-Garcia, J. C. Conesa, P. A. Midgley, X. Q. Wang, J. C. Hanson, J. A. Rodriguez, A. Marti-nez-Arias, *J. Phys. Chem. C* **2007**, *111*, 11026 – 11038; b) A. Hopkinson, D. A. King, *Chem. Phys.* **1993**, *177*, 433 – 452; c) T. Mallat, A. Baiker, *Appl. Catal. A* **2000**, *200*, 3 – 22.

[15] a) D. R. Baer, M. H. Engelhard, G. E. Johnson, J. Laskin, J. F. Lai, K. Mueller, P. Munusamy, S. Thevuthasan, H. F. Wang, N. Washton, A. Elder, B. L. Baisch, A. Karakoti, S. V. N. T. Kuchibhatla, D. Moon, *J. Vac. Sci. Technol. A* **2013**, *31*; b) M. A. Bañares, *Adv. Mater.* **2011**, *23*, 5293 – 5301; c) M. A. Bañares, I. E. Wachs, *J. Raman Spectrosc.* **2002**, *33*, 359 – 380; d) A. I. Frenkel, J. A. Rodriguez, J. G. Chen, *ACS Catal.* **2012**, *2*, 2269 – 2280; e) S. Lwin, I. E. Wachs, *ACS Catal.* **2014**, *4*, 2505 – 2520; f) A. M. Molenbroek, S. Helveg, H. Topsøe, B. S. Clausen, *Top. Catal.* **2009**, *52*, 1303 – 1311; g) J. A. Rodriguez, J. C. Hanson, D. Stacchiola, S. D. Senanayake, *Phys. Chem. Chem. Phys.* **2013**, *15*, 12004 – 12025; h) H. Topsøe, *J. Catal.* **2003**, *216*, 155 – 164; i) B. M. Weckhuysen, *Phys. Chem. Chem. Phys.* **2003**, *5*, 4351 – 4360.

[16] a) M. A. Bañares, *Catal. Today* **2005**, *100*, 71 – 77; b) S. Deabate, G. Gebel, P. Huguet, A. Morin, G. Pourcelly, *Energy Environ. Sci.* **2012**, *5*, 8824 – 8847; c) C. Sievers, S. R. Bare, E. Stavitski, *Catal. Today* **2013**, *205*, 1 – 2.

[17] a) K. Fottinger, J. A. van Bokhoven, M. Nachtegaal, G. Rupprechter, *J. Phys. Chem. Lett.* **2011**, *2*, 428 – 433; b) J. L. Fulton, J. C. Linehan, T. Autrey, M. Balasubramanian, Y. Chen, N. K. Szymczak, *J. Am. Chem. Soc.* **2007**, *129*, 11936 – 11949.

[18] J. Kulisch, H. Sommer, T. Brezesinski, J. Janek, *Phys. Chem. Chem. Phys.* **2014**, *16*, 18765 – 18771.

[19] S. J. Tinnemans, M. H. F. Kox, T. A. Nijhuis, T. Visser, B. M. Weckhuysen, *Phys. Chem. Chem. Phys.* **2005**, *7*, 211 – 216.

[20] a) A. M. Beale, A. M. J. van der Eerden, K. Kervinen, M. A. Newton, B. M. Weckhuysen, *Chem. Commun.* **2005**, 3015 – 3017; b) M. H. Groothaert, K.

[21] a) A. Goguet, F. C. Meunier, D. Tibiletti, J. P. Breen, R. Burch, *J. Phys. Chem. B* **2004**, *108*, 20240 – 20246; b) T. Lesage, C. Verrier, P. Bazin, J. Saussey, M. Daturi, *Phys. Chem. Chem. Phys.* **2003**, *5*, 4435 – 4440; c) O. Marie, F. Thibault-Starzyk, P. Massiani, *J. Catal.* **2005**, *230*, 28 – 37; d) G. Ramakrishnan, S. Zhao, W. Q. Han, A. Orlov, *Chem. Eng. J.* **2011**, *170*, 445 – 450; e) J. Sirita, S. Phanichphant, F. C. Meunier, *Anal. Chem.* **2007**, *79*, 3912 – 3918; f) S. Zhao, G. Ramakrishnan, D. Su, R. Rieger, A. Koller, A. Orlov, *Appl. Catal. B* **2011**, *104*, 239 – 244.

[22] a) M. E. Holtz, Y. C. Yu, D. Gunceler, J. Gao, R. Sundararaman, K. A. Schwarz, T. A. Arias, H. D. Abruna, D. A. Müller, *Nano Lett.* **2014**, *14*, 1453 – 1459; b) J. B. Leriche, S. Hamelet, J. Shu, M. Morcrette, C. Masque-lier, G. Ouvrard, M. Zerrouki, P. Soudan, S. Belin, E. Elkaim, F. Baudelet, *J. Electrochem. Soc.* **2010**, *157*, A606 – A610; c) M. Tada, S. Murata, T. Asako-ka, K. Hiroshima, K. Okumura, H. Tanida, T. Uruga, H. Nakanishi, S. Mat-sumoto, Y. Inada, M. Nomura, Y. Iwasawa, *Angew. Chem. Int. Ed.* **2007**, *46*, 4310 – 4315; *Angew. Chem.* **2007**, *119*, 4388 – 4393.

[23] a) S. J. Tinnemans, J. G. Mesu, K. Kervinen, T. Visser, T. A. Nijhuis, A. M. Beale, D. E. Keller, A. M. J. van der Eerden, B. M. Weckhuysen, *Catal. Today* **2006**, *113*, 3 – 15; b) W. Q. Xu, R. Si, S. D. Senanayake, J. Llorca, H. Idriss, D. Stacchiola, J. C. Hanson, J. A. Rodriguez, *J. Catal.* **2012**, *291*, 117 – 126.

[24] a) F. Tao, *ChemCatChem* **2012**, *4*, 583 – 590; b) M. A. van Spronsen, G. J. C. van Baarle, C. T. Herbschleb, J. W. M. Frenken, I. M. N. Groot, *Catal. Today* **2015**, *244*, 85 – 95.

[25] a) A. Patlolla, P. Baumann, W. Xu, S. D. Senanayake, J. A. Rodriguez, A. I. Frenkel, *Top. Catal.* **2013**, *56*, 896 – 904; b) S. Y. Yao, K. Mudiyanselage, W. Q. Xu, A. C. Johnston-Peck, J. C. Hanson, T. P. Wu, D. Stacchiola, J. A. Rodriguez, H. Y. Zhao, K. A. Beyer, K. W. Chapman, P. J. Chupas, A. Marti-nez-Arias, R. Si, T. B. Bolin, W. J. Liu, S. D. Senanayake, *ACS Catal.* **2014**, *4*, 1650 – 1661.

[26] S. J. L. Billinge, I. Levin, *Science* **2007**, *316*, 561 – 565.

[27] a) G. Kolb, V. Hessel, *Chem. Eng. J.* **2004**, *98*, 1 – 38; b) G. Kolb, V. Hessel, V. Cominos, C. Hofmann, H. Lowe, G. Nikolaidis, R. Zapf, A. Ziogas, E. R. Delsman, M. H. J. M. de Croon, J. C. Schouten, O. de La Iglesia, R. Malla-da, J. Santamaria, *Catal. Today* **2007**, *120*, 2 – 20; c) G. Sankar, E. H. Cao, A. Gavriilidis, *Catal. Today* **2007**, *125*, 24 – 28.

[28] a) S. Chenna, P. A. Crozier, *ACS Catal.* **2012**, *2*, 2395 – 2402; b) M. Gu, L. R. Parent, B. L. Mehdi, R. R. Unocic, M. T. McDowell, R. L. Sacci, W. Xu, J. G. Connell, P. H. Xu, P. Abellan, X. L. Chen, Y. H. Zhang, D. E. Perea, J. E. Evans, L. J. Lauhon, J. G. Zhang, J. Liu, N. D. Browning, Y. Cui, I. Arslan, C. M. Wang, *Nano Lett.* **2013**, *13*, 6106 – 6112; c) B. L. Mehdi, M. Gu, L. R. Parent, W. Xu, E. N. Nasybulin, X. L. Chen, R. R. Unocic, P. H. Xu, D. A. Welch, P. Abellan, J. G. Zhang, J. Liu, C. M. Wang, I. Arslan, J. Evans, N. D. Browning, *Microsc. Microanal.* **2014**, *20*, 484 – 492.

[29] S. I. Zabinsky, J. J. Rehr, A. Ankudinov, R. C. Albers, M. J. Eller, *Phys. Rev. B* **1995**, *52*, 2995 – 3009.

[30] J. Park, S. Heo, J. Chung, G. S. Park, *Microsc. Microanal.* **2013**, *19*, 109 – 113.

[31] A. Patlolla, E. V. Carino, S. N. Ehrlich, E. Stavitski, A. I. Frenkel, *ACS Catal.* **2012**, *2*, 2216 – 2223.

[32] a) I. M. Arabatzis, T. Stergiopoulos, D. Andreeva, S. Kitova, S. G. Neophy-tides, P. Falaras, *J. Catal.* **2003**, *220*, 127 – 135; b) P. Falaras, A. H. Le Goff, M. C. Bernard, A. Xagas, *Sol. Energy Mater. Sol. Cells* **2000**, *64*, 167 – 184.

[33] Y. Yu, J. C. Yu, J. G. Yu, Y. C. Kwok, Y. K. Che, J. C. Zhao, L. Ding, W. K. Ge, P. K. Wong, *Appl. Catal. A* **2005**, *289*, 186 – 196.

[34] H. L. L. Xin, K. Y. Niu, D. H. Alsem, H. M. Zheng, *Microsc. Microanal.* **2013**, *19*, 1558 – 1568.

[35] A. Kolmakov, D. A. Dikin, L. J. Cote, J. X. Huang, M. K. Abyaneh, M. Amati, L. Gregoratti, S. Gunther, M. Kiskinova, *Nat. Nanotechnol.* **2011**, *6*, 651 – 657.